Published in final edited form as:
J Phys Chem B. 2013 December 12; 117(49): . doi:10.1021/jp4064577.

Redox State Dependence of Axial Ligand Dynamics in *Nitrosomonas europaea* Cytochrome c_{552}

Ravinder Kaur[†] and **Kara L. Bren**[‡,*]

[†]Center for Infectious Disease and Immunology, Research Institute, Rochester General Hospital, Rochester, NY 14621

[‡]Department of Chemistry, University of Rochester, Rochester NY, 14627-0216

Abstract

Analysis of NMR spectra reveals that the heme axial Met ligand orientation and dynamics in *Nitrosomonas europaea* cytochrome c_{552} (*Ne* cyt *c*) are dependent on heme redox state. In the oxidized state, the heme axial Met is fluxional, interconverting between two conformers related to each other by inversion through the Met δS atom. In the reduced state, there is no evidence of fluxionality, with the Met occupying one conformation similar to that seen in the homologous *Pseudomonas aeruginosa* cytochrome c_{551}. Comparison of the observed and calculated pseudocontact shifts for oxidized *Ne* cyt *c* using the reduced protein structure as a reference structure reveals a redox-dependent change in the structure of the loop bearing the axial Met (loop 3). Analysis of nuclear Overhauser effects (NOEs) and existing structural data provides further support for the redox state dependence of loop 3 structure. Implications for electron transfer function are discussed.

Keywords

Nitrosomonas europaea; Cytochrome *c*; NMR; Pseudocontact shifts; Dynamics

INTRODUCTION

Electron transfer (ET) reactions between proteins are essential in energy transduction pathways.[1,2] Because biological ET reactions typically occur at low driving forces, minimizing reorganization energy is expected to increase ET rates in biological systems.[3] To minimize reorganization energy, it is proposed that ET metalloproteins suppress changes in structure associated with changes in metal redox state. Indeed, comparisons of the structures of oxidized and reduced ET proteins typically reveal only small changes in structure with redox state,[4–12] consistent with low reorganization energies and fast ET rates at low driving force.[13–17] To minimize reorganization energy, ET metalloproteins were traditionally assumed to be structurally rigid, particularly at the metal site.[13,18,19] In recent years, however, results of experimental and computational studies have revealed that ET metalloproteins are not as rigid as traditionally thought. In some ET metalloproteins, significant structural mobility has been observed near the metal site.[20–24] Contrary to the traditional view of a static redox site, mobility may play a role in ET gating, in docking to redox partners, and in modulating donor-acceptor distance and coupling.[25–33] The

[*]Corresponding Author: Department of Chemistry, University of Rochester, Rochester NY 14627-0216. bren@chem.rochester.edu; tel: 585-275-4335.

Supporting information. Additional NMR data, tables of pseudocontact shifts and chemical shift assignments. This material is available free of charge via the Internet at http://pubs.acs.org.

relationship between protein dynamics and ET activity is not fully understood but is evolving away from the concept that an ET protein acts as a rigid entity to the idea that dynamics play an active role in modulating biological ET reactions.

Here, we investigate the dependence on redox state of heme axial methionine dynamics in *Nitrosomonas europaea* cytochrome c_{552} (*Ne* cyt *c*). *Ne* cyt *c* belongs to the cyt c_8 family of small (~80 amino acids) bacterial cyts *c* with His/Met heme axial ligation, and has been noted for its unusual spectroscopic properties. For one, it displays a "large g_{max}"-type EPR spectrum, in contrast with the rhombic spectra seen for many cyts *c*.[34–37] In addition, the ^{1}H NMR spectrum of oxidized *Ne* cyt *c* shows an unusually small range of chemical shifts for its heme methyl resonances,[38] which has been proposed to result from fluxionality of the heme axial Met, in which the side chain interconverts between the "*R*" and "*S*" configurations rapidly on the NMR time scale (Figure 1).[21,39] Axial Met fluxionality has been observed in two other cytochromes to date, *Hydrogenobacter thermophilus* cytochrome c_{552} (*Ht* cyt *c*),[21] and the N64Q mutant of *Pa* cyt *c*,[40] which are also members of the cyt c_8 structural family.

In conflict with the proposal that the *Ne* cyt *c* axial Met is fluxional is the solution (NMR) structure of the reduced protein showing the axial methionine in a single conformation, and with an orientation similar to that seen in *Pa* cyt *c* (Figure 1A).[42] In support of the presence of Met fluxionality, however, is a recent X-ray crystal structure of *Ne* cyt *c* crystallized in the oxidized state that shows evidence of the axial Met occupying both *R* and *S* forms.[43] In this work, we investigate the basis for these seemingly contradictory results on *Ne* cyt *c* axial Met orientation and propose that the heme axial Met orientation and dynamics in *Ne* cyt *c* are dependent on heme redox state. Furthermore, the analysis herein reveals that the methionine-donating loop (loop 3; residues 50–68) in *Ne* cyt *c* undergoes a redox state-dependent change in structure that accompanies the change in axial methionine orientation and dynamics. Although small redox-linked changes in structure and in polypeptide dynamics have been noted before in cytochromes, a substantial change in axial ligand orientation with redox state has not previously been reported.

MATERIALS AND METHODS

Sample Preparation

Ne cyt *c* was expressed by growing BL21(DE3) cells harboring the pSNEC (Amp^r)[39] and pEC86 (Cm^r)[44] plasmids in LB medium supplemented with ampicillin (50 μg/mL) and chloramphenicol (50 μg/mL). The culture was agitated at 110 rpm at 37 °C for 16 h and the cells were harvested by centrifugation. Purification of *Ne* cyt *c* from cell pellets was as reported.[39] *Pa* cyt *c* was expressed and purified as described.[45] Horse cyt *c* was purchased from Sigma. The numbering system used herein for *Ne* cyt *c* is based on the *Pa* cyt *c* sequence, starting with residue 3 in *Ne* cyt *c* and placeing the axial His and Met ligands at positions 16 and 61, respectively.

NMR Spectroscopy

Proton NMR spectra were collected on a Varian INOVA 500-MHz spectrometer. *Ne* cyt *c* (1–3 mM) was in 50 mM sodium phosphate, pH 7.0 containing 10% D_2O. Ferric protein samples contained a 5-fold molar excess of $K_3[Fe(CN)_6]$. Ferrous protein samples were prepared by adding a 20–40-fold molar excess of $Na_2S_2O_4$ after bubbling nitrogen through the sample. For oxidized *Ne* cyt *c*, 2-D NOESY (mixing time 100 ms) and TOCSY (spin-lock time 90 ms) spectra were collected at 298 K with a 30,000-Hz spectral width, 4096 points in the F2 dimension, and 512 increments in the F1 dimension. 2-D NOESY and TOCSY spectra of ferric *Ne* cyt *c* were also collected at 303 K to resolve spectral overlap.

For ferrous *Ne* cyt *c*, NOESY and TOCSY spectra were taken with a 12,000-Hz spectral width, 4096 points in the F2 dimension, and 512 increments in the F1 dimension. Presaturation was used to suppress the solvent signal. For variable temperature (266–300 K) 1-D ^{1}H-NMR experiments, oxidized *Ne* cyt *c* was prepared in 50 mM sodium phosphate, pH 7.0, with 10% D_2O and 20% (v/v) CD_3OD.

Assignments of heme ^{1}H resonances of oxidized and reduced *Ne* cyt *c* were made by identifying connectivities between heme substituents in NOESY spectra according to standard procedures.[46] Polypeptide ^{1}H resonances were also assigned according to established methods[47] and were guided by published assignments.[39,42]

NMR Line Shape Analysis

For the analysis of the temperature dependence of heme methyl resonance line shapes for ferric *Ne* cyt *c*, ^{1}H NMR spectra were processed using the program NUTS 2001 (Acorn NMR, Inc.). The program WINDNMR (version 7.1.5) was used to simulate the heme 5-CH_3 and 8-CH_3 ^{1}H resonances; the 1-CH_3 and 3-CH_3 resonances were excluded from the analysis because of their overlap at lower temperatures. The following assumptions were made when carrying out the simulation:[21] 1) the exchange is between two states corresponding to axial Met configurations *R* and *S* (Figure 1A, B); 2) a population ratio of 1:1 for the two states is maintained; 3) the chemical shifts of the heme methyl resonances in configuration *S* are same as those of the corresponding resonances in *Pa* cyt *c* (Figure 1C), and 4) the natural line width of the *Ne* cyt *c* heme methyl resonances in the absence of exchange is the same as that of the corresponding resonances in *Pa* cyt *c*, which does not show axial Met dynamics. The values for the rate constant for exchange (k) and the chemical shifts for *Ne* cyt *c* with Met in configuration *R* are calculated in the simulation. An Eyring plot of $\ln(k/T)$ vs. $1/T$ was analyzed to determine activation parameters.

Determination of Magnetic Axes

Experimental pseudocontact shifts (δ_{pc}^{obs}) were determined by taking the difference between the observed chemical shift of a proton in the oxidized (δ_{ox}) and reduced (δ_{red}) states:

$$\delta_{pc}^{obs} = \delta_{ox} - \delta_{red} \quad [1]$$

The relationship in equation 1 assumes that the contact shift is negligible and that the protein undergoes no significant structural change with redox state. The contact shift contribution will be non-negligible only for iron-coordinated residues. Therefore, nuclei on the heme, the axial ligands, and Cys residues attached to the heme were excluded. The atomic coordinates of reduced *Ne* cyt *c* (PDB: 1A56)[42] were used in magnetic axes calculations for the purpose of identifying redox-linked structure change. The folds of oxidized and reduced *Ne* cyt *c* are known from structural determinations to be similar to each other overall.[42,43] A total of 167 pseudocontact shifts from throughout the protein structure are used in the calculation so that the calculation is based on shifts for residues both near to and relatively distant from the iron, and dispersed throughout the protein structure. The orientation of magnetic axes and the values of axial ($\Delta\chi_{rh}$) and rhombic ($\Delta\chi_{ax}$) magnetic anisotropies for oxidized *Ne* cyt *c* were determined using an in-house program[21] according to a published procedure.[48] First, molecular coordinates were defined with the heme iron at the origin, the +*z* axis perpendicular to the mean plane of the heme pyrrole nitrogen atoms in the direction of axial Met, and the +*y* axis aligned along the direction of the pyrrole I nitrogen (Figure 2). Next, the protein structure was rotated in a stepwise fashion and at each step a least-squares fitting of experimental pseudocontact shifts to equation 2 was performed:

$$\delta_{pc,i}{}^{obs}=(1/12\pi r^3)[\Delta\chi_{ax}(3n_i{}^2-1)+(3/2)\,\Delta\chi_{rh}(l_i{}^2-m_i{}^2)] \quad [2]$$

where r_i is the distance from the iron to atom *i* (determined from the three-dimensional structure), and l_i, m_i, and n_i are the direction cosines of the position vector of atom *i* (r_i) with respect to the magnetic axes.[49] The sum-squared error between calculated and experimental pseudocontact shifts was used to assess the goodness of fit. Experimental pseudocontact shifts used in the fit are reported in Table S1 in supporting information.

RESULTS AND DISCUSSION

Heme Methyl Resonance Line Shapes and Chemical Shifts

It was previously reported that the 1-D NMR spectrum of oxidized *Ne* cyt *c* displays an unusual pattern of resonances in the high-frequency region, with all four heme methyls having similar shifts to each other, giving a spread of only 4.1 ppm at 298 K (Figure 1E).[38,39] This finding contrasts with the typically large spread seen for heme methyl shifts in ferric heme proteins with His-Met axial ligation of ~ 20 – 30 ppm (Figure 1C,D).[50] The compression of the heme methyl shifts in *Ne* cyt *c* is consistent with exchange of the heme axial Met between configurations *R* and *S* (Figure 1A,B) rapidly on the NMR time scale.[21,39] The pattern of heme methyl chemical shifts for configuration *R* has methyls 3-CH_3 and 8-CH_3 with higher chemical shifts relative to 5-CH_3 and 1-CH_3, whereas for configuration *S* methyls 5-CH_3 and 1-CH_3 have higher chemical shifts relative to 8-CH_3 and 1-CH_3. Upon rapid exchange, the observed chemical shifts are the average of those seen for these two orientations, giving similar chemical shifts for all four heme methyls. Along with the chemical shift pattern, the temperature-dependent properties of the *Ne* cyt *c* NMR spectrum, reported previously,[39] are consistent with axial Met fluxionality. At low temperature (266 K), the heme methyl ^{1}H NMR resonances of *Ne* cyt *c* exhibit line widths > 500 Hz, over four-fold greater that those seen in the spectrum at 300 K, and similar to what is seen for *Ht* cyt *c*, which has a fluxional Met.[21] In contrast, in *Pa* cyt *c* over this temperature range, line widths show little change. This increase in line width observed in *Ne* cyt *c* as temperature decreases does not correlate with changes in the T_1 values for the heme methyls, indicating that the temperature-dependent process responsible for the increase in line width is not the electron relaxation time. A candidate is a chemical exchange process that affects the chemical shifts of all four heme methyls, i.e., fluxionality of the axial Met.[21,39] An analogous motion of the axial His is unlikely because its orientation is essentially fixed by the *c*-heme-binding motif.[51,52] Also in support of this exchange process is the X-ray crystal structure of ferric *Ne* cyt *c* isolated from *N. europaea* cells that was determined recently. A structure was determined with 18 molecules in the asymmetric unit; of these molecules, 14 display the axial Met in the *S* orientation, and 4 could be refined with either orientation, suggesting a mixture of *S* and *R* orientations for those molecules. Thus the X-ray crystal structure lends further support for the presence of Met fluxionality in oxidized *Ne* cyt *c* observed by NMR. However, it is important to note that there is evidence of photoreduction of the protein during X-ray diffraction data collection, resulting in ambiguity of the oxidation state in the crystal structure.[43]

To determine the rate of axial Met exchange, simulation of the heme 5-CH_3 and 8-CH_3 resonances in the *Ne* cyt *c* NMR spectrum using WINDNMR has been performed. The chemical shifts calculated for configuration *R* (17.37 ppm for 5-CH_3 and 30.16 ppm for 8-CH_3 at −7 °C) are consistent with this orientation because they are similar to measured values for oxidized horse cyt *c* (13.17 ppm for 5-CH_3 and 38.40 ppm for 8-CH_3 at −7 °C), which has Met configuration *R*. The shifts for configuration *S*, which are assumed in this analysis to be the same as those for *Pa* cyt *c*, and the observed shifts for *Ne* cyt *c*, assumed to be the average of *R* and *S*, were inputs in this calculation. The spectra resulting from the

simulation and the determined exchange rates are shown in Figure 3. The excellent agreement between the simulated and experimental spectra provides further support for the existence of Met fluxionality in this protein. The activation enthalpy for the exchange process determined from an Eyring plot was determined to be 40 ± 2 kJ mol^{-1} (Supporting Figure S1), a value that is similar to that determined for small inorganic complexes in which thioether ligands undergo inversion at sulfur.[53–55] This $\Delta^{H\ddagger}$ value is somewhat smaller than that determined for Met fluxionality in *Ht* cyt *c* (59 ± 10 kJ/mol).[21]

Magnetic Axes and Axial Met Orientation in Ferric *Ne* cyt *c*

The orientation of the magnetic axes was determined for two reasons: 1) To evaluate the orientations of the axial ligands, 2) To determine whether the protein structure changes with redox state. The chemical shifts for oxidized and reduced *Ne* cyt *c* are reported in Tables S2 and S3, respectively. A total of 167 pseudocontact shifts were determined according to equation 1 and are reported in Table S1. From the pseudocontact shifts, the orientation and anisotropy of the paramagnetic susceptibility $^{tensor}\chi$ for oxidized *Ne* cyt *c* were determined by a least-squares fitting to equation 2, yielding results reported in Table 1 along with the values for *Pa* cyt *c* for comparison.[21] In cyts *c* the axial His orientation is typically held constant along the α-γ meso axis of the heme because of the constraints of the CXXCH motif,[51,52,56] hence differences in χ tensor orientation are expected to be primarily determined by axial Met orientation.[57] The small magnitude of the Euler angle β (the *z* axis tilt from *z′*, the heme normal) indicates that the *z* axis is nearly perpendicular to the heme plane, as expected.[21,48] When the *z* axis is perpendicular to the heme, the in-plane rotation of the magnetic axes relative to molecular axes is well defined by κ = α + γ. Relative to *Pa* cyt *c*, *Ne* cyt *c* displays an altered value of κ, which is related to the mean plane of the axial ligands relative to the heme, φ, according to φ = −κ, in a relationship known as the counterrotation rule.57 The −36° value of κ for *Ne* cyt *c* is similar to the value for the N64Q mutant of *Pa* cyt *c* (−38°)[40] and for *Ht* cyt *c* (−47°),[21] which have been shown to have fluxional Met ligands. In contrast, a value of −12° has been determined for *Pa* cyt *c*, which has a φ value of 16° as measured from the crystal structure.[21] This result, along with the line shape analysis reported above,[39] support the existence of Met fluxionality in oxidized *Ne* cyt *c*, similar to what is observed for oxidized *Ht* cyt *c*.[21,39]

In addition to the difference in κ, *Ne* cyt *c* displays differences in magnetic anisotropy relative to *Pa* cyt *c*. The rhombicity of the χ tensor ($\Delta\chi_{rh}/\Delta\chi_{ax}$) for *Ne* cyt *c* (0.13) is smaller than that previously determined by NMR for *Pa* cyt *c* (0.38).[21] These results from NMR are consistent with EPR analysis indicating rhombicity of 0.16 for *Ne* cyt *c* and 0.37 for *Pa* cyt *c*.[35] In the case of cytochromes with bis-His heme axial ligation, rhombicity is determined primarily by the angle formed by the ring planes of the two axial His.[58] In the case of hemes with His-Met axial ligation, no clear relationship between the magnetic anisotropy and axial ligand orientations has emerged.[36,37,43]

Axial Met Orientation in Ferrous *Ne* cyt *c*

The orientation of the axial Met ε-CH_3 relative to the porphyrin in reduced diamagnetic cytochromes is readily deduced by detection of NOEs between the Met ε-CH_3 protons and the porphyrin meso protons. In *Pa* cyt *c* (Met configuration *S* observed in the crystal structure), strong NOESY cross peaks are expected between the ε-CH_3 of axial Met and the heme γ-meso and δ-meso protons, but not to the α-meso proton. In Met configuration *R*, cross peaks to the heme δ-meso and α-meso, but not to the γ-meso proton are expected (Figure 1A, B). In reduced *Ne* cyt *c*, NOEs to the γ-meso and δ-meso protons, and to no other heme meso protons are observed (Figure 4), indicating that the position of the Met ε-CH_3 relative to the heme is similar to that seen for *Pa* cyt *c*. This observation is reflected by the NMR structure of reduced *Ne* cyt *c*, which has a axial Met orientation similar to that of

Pa cyt *c*.[42] These results support the conclusion that in reduced *Ne* cyt *c*, only one orientation of the axial Met is present, which is similar to that seen in *Pa* cyt *c*. We thus propose that in *Ne* cyt *c*, axial Met fluxionality is present in the oxidized state but not in the reduced state. This finding contrasts with the behavior of *Pa* cyt *c*, which displays a fixed Met orientation in both oxidation states,[4] and with *Ht* cyt *c* for which there is evidence of more than one axial Met orientation in both redox states.[21] Note that analysis of NOEs is not used here for evaluation of the axial Met conformation for the oxidized protein because the short T_1 values lead to loss of NOE intensity.

Evaluation of redox-linked structure change in *Ne* cyt *c*

The finding that the axial Met is fluxional in oxidized but not reduced *Ne* cyt *c* is unprecedented. This interesting redox-dependent behavior could be a result of a weaker Met(δS)-Fe(III) bond relative to a Met(δS)-Fe(II) bond,[59] lowering the barrier for fluxionality. Another explanation is that *Ne* cyt *c* undergoes a structural rearrangement upon oxidation state change that promotes Met ligand dynamics in the oxidized state. In support of this proposal, distal heme pocket mutations have been shown to alter heme axial Met dynamics in related cytochromes.[40,60] Aiding evaluation of redox-linked structure change are the three-dimensional structures of *Ne* cyt *c*. The structure of the protein crystallized in the oxidized form has been characterized through X-ray crystallography (PDB: 4JCG and 3ZOW),[43] and the NMR solution structure of the reduced protein has been reported (PDB: 1A56).[42] Alignment of the backbone atoms of the mean NMR structure of reduced *Ne* cyt *c* with the X-ray crystal structure of oxidized *Ne* cyt *c* is shown in Figure 5. Examination of the aligned structures reveals significant differences in loop 3; the backbone from residues 65–67 shows a particularly pronounced difference. Furthermore, the contact between Val23 and Ile59, which is at the bend of loop 3, is disrupted in the oxidized protein. In the X-ray crystal structure of oxidized *Ne* cyt *c* crystallized in the $P6_522$ space group PDB: 4JCG), the axial Met is found in only one orientation in each of the 4 molecules in the asymmetric unit, corresponding to configuration *S*. However, in a 2.35-Å structure of oxidized *Ne* cyt *c* crystallized in the $P2_12_12_1$ space group (PDB: 3ZOW), two Met orientations are observed among the 18 molecules in the asymmetric unit, consistent with fluxionality.[43] In comparing the 3-D structures of oxidized and reduced *Ne* cyt *c*, it is important to note that the comparison being made between the oxidized and reduced protein structures is between structures determined using two different methods, which may contribute to apparent structure differences. Furthermore, there is evidence that iron reduction occurs during X-ray data collection, and as a result the X-ray crystal structure of protein crystallized when oxidized may reflect a mixture of oxidation states.[43] Finally, a possible explanation for the single Met orientation in one of the X-ray crystal structures (4JCG) is the depletion of conformers present at room temperature upon cooling for data collection.[61,62] Thus, while comparison of the X-ray crystal structure to the NMR structure points to a change in the structure of loop 3, further evaluation of the structure in solution is warranted to test the hypothesis that structure changes with redox state.

To evaluate redox-dependent structure in solution, the results from the magnetic axes determination for oxidized *Ne* cyt *c* using the reduced *Ne* cyt *c* structure as a reference structure were examined. An assumption made in the determination of the magnetic axes using the method described here is that the oxidized and reduced proteins are isostructural. Thus, a significant difference in structure between the oxidized form and the reduced form will result in a deviation between calculated and observed pseudocontact shifts. Indeed, analysis of the plots of the δ_{pc}^{obs} vs. δ_{pc}^{calc} for *Ne* cyt *c* reveals a number of data points that deviate significantly from a line of slope 1 (Figure 6A). This scatter could arise from a number of factors including inaccuracies in the reference structure, incorrect assignments, or a difference in structure between the reduced reference state and the oxidized state.

However, it is notable that most of the points that deviate significantly from the linear correlation between the observed and calculated shifts for *Ne* cyt *c* (difference between observed and calculated is > 0.5 ppm) are in loop 3 (Gly51, Ser52, Ser53, Val55, Trp56, Pro60, and Asn64) or in contact with this loop (Val23). This finding is in support of a redox-dependent structural change in occurring in loop 3.

To further investigate the existence of a redox-linked structure change, NOEs involving residues in loop 3 in oxidized and reduced *Ne* cyt *c* were compared. Because of the enhanced nuclear relaxation in the oxidized form of the protein, the interpretation of loss of an NOE in the oxidized protein relative to the reduced protein is complicated by the possibility that the intensity loss results from the shorter T_1 values in the oxidized protein rather than an increase in internuclear distance relative to the reduced protein. Thus we consider only NOEs present in the oxidized and absent in the reduced protein as indications of a redox-linked structure change. The most notable difference between NOEs in the two redox states is that the amide proton of Gly50 displays NOEs to Hα and Hβ of Asn64 in the oxidized form (Figure S2), while in the reduced protein the Gly50 amide proton has no cross-peaks to the Asn64 side chain. Residues Asn64 and Gly50 sit across from each other within loop 3; disruption of these NOEs upon reduction would reflect a change in the loop conformation. Relevant to understanding the effect on the axial Met, in structures of *Ne* cyt *c* as well as its homologue *Pa* cyt *c*, the Asn64 side chain forms a hydrogen bond with Met61 δS; a change in this interaction resulting from a loop 3 rearrangement may influence Met orientation and dynamics. Indeed, mutation of residue 64 has been shown to alter Met orientation and dynamics in homologous proteins.[40,60,63] Analysis of the three-dimensional structures, however, suggests that the Asn64-Met61 contact remains intact in both oxidation states: The Asn64 δN is within H-bonding distance of the Met61 δS in the X-ray crystal structure (4JCG) of oxidized *Ne* cyt *c* (3.6 Å distance between heavy atoms), while in the NMR structure of reduced protein (1A56) this distance appears shorter (3.3 Å). Chemical shifts provide additional support for the presence of this contact in both oxidation states, aided by comparison to data for *Pa* cyt *c*, for which the Asn64 δNH to Met61 δS distance remains ~3.6 Å in both oxidation states.[4] In reduced *Ne* cyt *c*, one Asn64 δNH has a chemical shift (δ_{obs} = 3.43 ppm) consistent with a strong ring current shift and thus with its position near the Met61 δS above the heme plane. This shift is similar to that seen in *Pa* cyt *c* (δ_{obs} = 3.18 ppm).[40] In oxidized *Ne* cyt *c*, the Asn δNH protons (δ_{obs} = 12.15, 11.44 ppm) display large chemical shifts, on the order of those of oxidized *Pa* cyt *c* (δ_{obs} = 13.46, 13.86 ppm).[40] The large hyperfine shifts observed for these nuclei are consistent with the residue being positioned above the heme plane, near the Met61 side chain. Thus, surprisingly, it appears that there is minimal change in the contact between Asn64 and Met61 in *Ne* cyt *c* as a function of redox state, although there is strong support for the proposal that loop 3 conformation overall is sensitive to redox state.

Functional Implications

ET proteins typically undergo minimal structure change upon redox state change. Cytochromes *c* in particular have been reported to show only small changes in the hydrogen bonding network in the heme pocket, reorientation of heme propionates, and changes in positions of structural water upon redox state change.[4,6,7,10] The most well-studied systems are the mitochondrial cytochromes *c*, in which a number of studies have identified small redox-dependent changes in the hydrogen-bonding network near the heme, in heme propionate-7 orientation and hydrogen bonding, in Gly41, and in internal water molecules.[5,64,65] *Pa* cyt *c* shows similar small redox-dependent structure changes.[4] The most notable redox-dependent changes in *Pa* cyt *c* structure are movement of an internal water molecule and of Ile59. Notably, Ile59 forms a hydrophobic contact with Val23 (Figure 5), and a redox-dependent structure change in this contact is detected here in *Ne* cyt *c*.

The finding that *Ne* cyt *c* undergoes a change in axial Met orientation upon redox state change is surprising, as any change to the iron coordination sphere would be expected to increase reorganization energy for ET and thus decrease rates of ET reactions with redox partners at low driving force. However, in a study of the rates of ET reaction between structurally homologous bacterial cyts *c* with similar redox potentials (*Ne* cyt *c*, *Pa* cyt *c*, *P. stutzeri* cyt c_{551}, and *P. stutzeri ZoBell* cyt c_{551}) with the *P. stutzeri ZoBell* reductase, *Ne* cyt *c* displays a substantially (2-fold) higher rate for ET than the other cytochromes, which show rates similar to each other.[38] Additional studies would be needed to understand how this redox-dependent change in *Ne* cyt *c* structure influences reorganization energy. The change in ligand dynamics observed here, however, has some precedent in that changes in overall polypeptide dynamics with cytochrome *c* redox state are well-documented, with cyts *c* showing significantly more mobility in the oxidized relative to the reduced state.[10,11,65–67] It is likely that a similar change in polypeptide mobility occurs in *Ne* cyt *c*, and any such change may be related to the change in axial ligand mobility.

There are now a number of examples of redox-linked structure changes in metalloproteins with proposed or demonstrated functional relevance. For example, NMR studies of human ferredoxin reveal a change in secondary structure with redox state that is proposed to alter the affinity for ferredoxin reductase.[68] Similarly, in Anabaena ferredoxin a redox-dependent structural change in a loop is proposed to modulate the formation and dissociation of the electron-transfer complex between ferredoxin and ferredoxin NADP+ reductase.[69] A particularly well-characterized system is *Pseudomonas putida* putidaredoxin / cytochrome P450cam (Pdx/P450). Backbone dynamics of P450 are dependent on redox state, particularly in the protein region that interacts with Pdx, and these changes are proposed to regulate the formation and dissociation of the Pdx-P450 complex. Pdx binding also influences P450 structure and activity.[23,70] Furthermore, Pdx displays redox-dependent structure and dynamics that influence its interaction with P450.[71] Among multiheme cytochromes *c*, redox-linked structure changes have been identified that influence cooperativity of multielectron transfer[72] as well as proton-coupled ET.[73] Given the precedent provided by other redox proteins, the significant redox-dependent change in structure and ligand dynamics of *Ne* cyt *c* is expected to have functional relevance. *Ne* cyt *c* is present at high levels in *N. europaea* cells and is proposed to engage in ET with a number of partners including cytochrome c_{554}, diheme cytochrome *c* peroxidase, cytochrome bc_1, and nitrite reductase.[74,75] It is possible that its redox-dependent characteristics aid in regulating its binding to and release from multiple redox partners that include electron donors and acceptors. The determination of structures of complexes of *Ne* cyt *c* with known or potential redox partners would be valuable for determining whether the phenomena observed here are exploited by nature to regulate ET flow.

CONCLUSIONS

In this study, a redox-linked change in structure of the ET protein *Ne* cyt *c* has been identified by analysis of pseudocontact shifts and NOEs along with three-dimensional structures reported in the literature. The change in structure primarily involves the loop bearing the heme axial Met ligand, and is accompanied by an unusual change in the heme axial Met interaction with heme, with the Met becoming fluxional in the oxidized state. This result reveals more complex redox-dependent behavior of cytochromes than has previously been described, and is expected to have functional implications for ET reactions involving this cytochrome. Because of a paucity of structural data on protein-protein complexes of ET partners, factors that control specificity of biological ET reactions remain poorly understood.[76] Given its redox-dependent behavior, available high-resolution structures,[43] well-characterized electronic structure,[36,77,78] and multiple putative redox partners, *Ne* cyt *c*

constitutes an excellent model system for investigating the complex factors controlling biological ET reactions.

Supplementary Material

Refer to Web version on PubMed Central for supplementary material.

Acknowledgments

This work was supported by NIH grant R01-GM63170 to K.L.B.

References

1. Gray HB, Winkler JR. Electron Tunneling through Proteins. Q Rev Biophys. 2003; 36:341–372. [PubMed: 15029828]
2. Page CC, Moser CC, Dutton PL. Mechanism for Electron Transfer within and between Proteins. Curr Opin Chem Biol. 2003; 7:551–556. [PubMed: 14580557]
3. Marcus RA, Sutin N. Electron Transfers in Chemistry and Biology. Biochim Biophys Acta. 1985; 811:265–322.
4. Matsuura Y, Takano T, Dickerson RE. Structure of Cytochrome *c*-551 from *Pseudomonas aeruginosa* Refined at 1.6-Å Resolution and Comparison of the 2 Redox Forms. J Mol Biol. 1982; 156:389–409. [PubMed: 6283101]
5. Gao Y, Boyd J, Pielak GJ, Williams RJP. Proton Nuclear Magnetic Resonance as a Probe of Differences in Structure between the C102T and F82S, C102T Variants of Iso-1-Cytochrome *c* from the Yeast *Saccharomyces cerevisiae*. Biochemistry. 1991; 30:7033–7040. [PubMed: 1648968]
6. Berghuis AM, Brayer GD. Oxidation State Dependent Conformational Changes in Cytochrome*c*. J Mol Biol. 1992; 223:959–976. [PubMed: 1311391]
7. Zhao DZ, Hutton HM, Gooley PR, MacKenzie NE, Cusanovich MA. Redox-Related Conformational Changes in *Rhodobacter capsulatus* Cytochrome *c*(2). Protein Sci. 2000; 9:1828–1837. [PubMed: 11045628]
8. Guss JM, Harrowell PR, Murata M, Norris VA, Freeman HC. Crystal-Structure Analyses of Reduced (Cu^{I}) Poplar Plastocyanin at 6 pH Values. J Mol Biol. 1986; 192:361–387. [PubMed: 3560221]
9. Shepard WEB, Anderson BF, Lewandoski DA, Norris GE, Baker EN. Copper Coordination Geometry in Azurin Undergoes Minimal Change on Reduction of Copper(II) to Copper(I). J Am Chem Soc. 1990; 112:7817–7819.
10. Bartalesi I, Bertini I, Rosato A. Structure and Dynamics of Reduced *Bacillus pasteurii* Cytochrome *c*: Oxidation State Dependent Properties and Implications for Electron Transfer Processes. Biochemistry. 2003; 42:739–745. [PubMed: 12534286]
11. Banci L, Bertini I, Huber JG, Spyroulias GA, Turano P. Solution Structure of Reduced Horse Heart Cytochrome*c*. J Biol Inorg Chem. 1999; 4:21–31. [PubMed: 10499099]
12. Volkov AN, Vanwetswinkel S, Van de Water K, van Nuland NAJ. Redox-Dependent Conformational Changes in Eukaryotic Cytochromes Revealed by Paramagnetic NMR Spectroscopy. J Biomol NMR. 2012; 52:245–256. [PubMed: 22318343]
13. Vallee BL, Williams RJP. Metalloenzymes: The Entatic Nature of Their Active Sites. Proc Natl Acad Sci US A. 1968; 59:498–505.
14. Churg AK, Weiss RM, Warshel A, Takano T. On the Action of Cytochrome *c*- Correlating Geometry Changes Upon Oxidation with Activation Energies of Electron Transfer. J Phys Chem. 1983; 87:1683–1694.
15. Nocera DG, Winkler JR, Yocom KM, Bordignon E, Gray HB. Kinetics of Intramolecular Electron-Transfer from Ru(II) to Fe(III) in Ruthenium-Modified Cytochrome*c*. J Am Chem Soc. 1984; 106:5145–5150.
16. Andrew SM, Thomasson KA, Northrup SH. Simulation of Electron-Transfer Self-Exchange in Cytochrome *c* and Cytochrome *b*(5). J Am Chem Soc. 1993; 115:5516–5521.

17. Muegge I, Qi PX, Wand AJ, Chu ZT, Warshel A. The Reorganization Energy of Cytochrome *c* Revisited. J Phys Chem B. 1997; 101:825–836.
18. Gray HB, Malmstrom BG, Williams RJP. Copper Coordination in Blue Proteins. J Biol Inorg Chem. 2000; 5:551–559. [PubMed: 11085645]
19. Malmström BG. Rack-Induced Bonding in Blue-Copper Proteins. Eur J Biochem. 1994; 223:711–718. [PubMed: 8055947]
20. Zaballa ME, Abriata LA, Donaire A, Vila AJ. Flexibility of the Metal-Binding Region in Apo-Cupredoxins. Proc Natl Acad Sci US A. 2012; 109:9254–9259.
21. Zhong L, Wen X, Rabinowitz TM, Russell BS, Karan EF, Bren KL. Heme Axial Methionine Fluxionality in *Hydrogenobacter Thermophilus* Cytochrome *c*-552. Proc Natl Acad Sci US A. 2004; 101:8637–8642.
22. Zhuravleva AV, Korzhnev DM, Kupce E, Arseniev AS, Billeter M, Orekhov VY. Gated Electron Transfers and Electron Pathways in Azurin: A NMR Dynamic Study at Multiple Fields and Temperatures. J Mol Biol. 2004; 342:1599–1611. [PubMed: 15364584]
23. Pochapsky SS, Dang M, OuYang B, Simorellis AK, Pochapsky TC. Redox-Dependent Dynamics in Cytochrome P450(cam). Biochemistry. 2009; 48:4254–4261. [PubMed: 19366254]
24. Lyons TA, Ratnaswamy G, Pochapsky TC. Redox-Dependent Dynamics of Putidaredoxin Characterized by Amide Proton Exchange. Protein Sci. 1996; 5:627–639. [PubMed: 8845752]
25. Jeuken LJC. Conformational Reorganisation in Interfacial Protein Electron Transfer. Biochim Biophys Acta. 2003; 1604:67–76. [PubMed: 12765764]
26. Liang ZX. Dynamic Docking and Electron Transfer between Zn-Myoglobin and Cytochrome *b*(5). J Am Chem Soc. 2002; 124:6849–6859. [PubMed: 12059205]
27. Michel LV, Bren KL. Submolecular Unfolding Units of *Pseudomonas aeruginosa* Cytochrome *c*-551. J Biol Inorg Chem. 2008; 13:837–845. [PubMed: 18392863]
28. Daizadeh I, Medvedev ES, Stuchebrukhov AA. Effect of Protein Dynamics on Biological Electron Transfer. Proc Natl Acad Sci US A. 1997; 94:3703–3708.
29. Balabin IA, Onuchic JN. Dynamically Controlled Protein Tunneling Paths in Photosynthetic Reaction Centers. Science. 2000; 290:114–117. [PubMed: 11021791]
30. Massari AM, McClain BL, Finkelstein IJ, Lee AP, Reynolds HL, Bren KL, Fayer MD. Cytochrome *c* Mutants: Structure and Dynamics at the Active Site Probed by Multidimensional NMR and Vibration Echo Spectroscopy. J Phys Chem B. 2006; 110:18803–18810. [PubMed: 16986870]
31. Ubbink M. Dynamics in Transient Complexes of Redox Proteins. Biochem Soc Trans. 2012; 40:415–418. [PubMed: 22435822]
32. Galinato MGI, Kleingardner JG, Bowman SEJ, Alp EE, Zhao J, Bren KL, Lehnert N. Heme-Protein Vibrational Couplings in Cytochrome *c* Provide a Dynamic Link That Connects the Heme-Iron and the Protein Surface. Proc Natl Acad Sci US A. 2012; 109:8896–8900.
33. Kundu P, Dua A. Protein Dynamics Modulated Electron Transfer Kinetics in Early Stage Photosynthesis. J Chem Phys. 2013; 138:045104–045104. [PubMed: 23387626]
34. Walker FA. Magnetic Spectroscopic (EPR, ESEEM, Mössbauer, MCD and NMR) Studies of Low-Spin Ferriheme Centers and Their Corresponding Heme Proteins. Coord Chem Rev. 1999; 186:471–534.
35. Arciero DM, Peng QY, Peterson J, Hooper AB. Identification of Axial Ligands of Cytochrome *c*-552 from *Nitrosomonas europaea*. FEBS Lett. 1994; 342:217–220. [PubMed: 8143881]
36. Zoppellaro G, Harbitz E, Kaur R, Ensign AA, Bren KL, Andersson KK. Modulation of the Ligand-Field Anisotropy in a Series of Ferric Low-Spin Cytochrome *c* Mutants Derived from *Pseudomonas aeruginosa* Cytochrome *c*-551 and *Nitrosomonas europaea* Cytochrome *c*-552: A Nuclear Magnetic Resonance and Electron Paramagnetic Resonance Study. J Am Chem Soc. 2008; 130:15348–15360. [PubMed: 18947229]
37. Zoppellaro G, Bren KL, Ensign AA, Harbitz E, Kaur R, Hersleth HP, Ryde U, Hederstedt L, Andersson KK. Studies of Ferric Heme Proteins with Highly Anisotropic/Highly Axial Low Spin (*S*=1/2) Electron Paramagnetic Resonance Signals with Bis-Histidine and Histidine-Methionine Axial Iron Coordination. Biopolymers. 2009; 91:1064–1082. [PubMed: 19536822]

38. Timkovich R, Cai ML, Zhang BL, Arciero DM, Hooper AB. Characteristics of the Paramagnetic 1h Nmr Spectra of the Ferricytochrome *c*-551 Family. Eur J Biochem. 1994; 226:159–168. [PubMed: 7957244]
39. Bren KL, Kellogg JA, Kaur R, Wen X. Folding, Conformational Changes, and Dynamics of Cytochromes *c* Probed by NMR Spectroscopy. Inorg Chem. 2004; 43:7934–7944. [PubMed: 15578827]
40. Wen X, Bren KL. Heme Axial Methionine Fluxion in *Pseudomonas aeruginosa* Asn64Gln Cytochrome *c*-551. Inorg Chem. 2005; 44:8587–8593. [PubMed: 16271000]
41. Bushnell GW, Louie GV, Brayer GD. High-Resolution 3-Dimensional Structure of Horse Heart Cytochrome *c*. J Mol Biol. 1990; 214:585–595. [PubMed: 2166170]
42. Timkovich R, Bergmann D, Arciero DM, Hooper AB. Primary Sequence and Solution Conformation of Ferrocytochrome *c*-552 from *Nitrosomonas europaea*. Biophys J. 1998; 75:1964–1972. [PubMed: 9746537]
43. Can M, Krucinska J, Zoppellaro G, Andersen NH, Wedekind JE, Hersleth H-P, Andersson KK, Bren KL. Structural Characterization of *Nitrosomonas europaea* Cytochrome *c*-552 Variants with Marked Differences in Electronic Structure. Chem Bio Chem. 2013 in press.
44. Arslan E, Schulz H, Zufferey R, Kunzler P, Thöny-Meyer L. Overproduction of the *Bradyrhizobium japonicum c*-Type Cytochrome Subunits of the *cbb*(3) Oxidase in *Escherichia coli*. Biochem Biophys Res Commun. 1998; 251:744–747. [PubMed: 9790980]
45. Russell BS, Zhong L, Bigotti MG, Cutruzzolà F, Bren KL. Backbone Dynamics and Hydrogen Exchange of *Pseudomonas aeruginosa* Ferricytochrome *c*-551. J Biol Inorg Chem. 2003; 8:156–166. [PubMed: 12459911]
46. La Mar, GN.; de Ropp, JS. Biological Magnetic Resonance: NMR of Paramagnetic Molecules. Berliner, LJ.; Reuben, J., editors. Vol. 12. Plenum Press; New York: 1993. p. 1-78.
47. Wüthrich, K. NMR of Proteins and Nucleic Acids. Wiley; New York: 1986.
48. Emerson SD, La Mar GN. NMR Determination of the Orientation of the Magnetic Susceptibility Tensor in Cyanometmyoglobin - a New Probe of Steric Tilt of Bound Ligand. Biochemistry. 1990; 29:1556–1566. [PubMed: 2334714]
49. La Mar, GN.; Satterlee, JD.; de Ropp, JS. The Porphyrin Handbook. Kadish, KM.; Smith, KM.; Ruilard, R., editors. Vol. 5. Academic Press; New York: 2000. p. 185-298.
50. Shokhirev NV, Walker FA. The Effect of Axial Ligand Plane Orientation on the Contact and Pseudocontact Shifts of Low-Spin Ferriheme Proteins. J Biol Inorg Chem. 1998; 3:581–594.
51. Low DW, Gray HB, Duus JØ. Paramagnetic NMR Spectroscopy of Microperoxidase-8. J Am Chem Soc. 1997; 119:1–5.
52. Fufezan C, Zhang J, Gunner MR. Ligand Preference and Orientation in *b*- and *c*-Type Heme-Binding Proteins. Proteins. 2008; 73:690–704. [PubMed: 18491383]
53. Tresoldi G, Lo Schiavo S, Lanza S, Cardiano P. A Congested Ru(dps)(2) or Ru(dprs)(2) Core (dps = di-2-pyridyl sulfide; dprs = di-2-pyrimidinyl sulfide) Promotes Sulfur Inversion of N,S-Chelate Thioethers Containing CH_2R and 2-Pyridyl or 2-Pyrimidinyl Groups. Eur J Inorg Chem. 2002:181–191.
54. Shan XP, Espenson JH. Kinetics and Mechanisms of Reactions of Reo(kappa(2)-edt)(kappa(2)-edtme): Phosphane Displacement of the Thioether Group and Inversion of the Thioether Sulfur. Organometallics. 2003; 22:1250–1254.
55. Canovese L, Lucchini V, Santo C, Visentin F, Zambon A. A Novel Mechanism for the Fluxional Behaviour of Pd(eta(2)-tetramethylethylenetetracarboxylate)(2-methylthiomethylpyridine). J Organomet Chem. 2002; 642:58–63.
56. Bowman SEJ, Bren KL. The Chemistry and Biochemistry of Heme *c*: Functional Bases for Covalent Attachment. Nat Prod Rep. 2008; 25:1118–1130. [PubMed: 19030605]
57. Shokhirev NV, Walker FA. Co- and Counterrotation of Magnetic Axes and Axial Ligands in Low-Spin Ferriheme Systems. J Am Chem Soc. 1998; 120:981–990.
58. Yatsunyk LA, Dawson A, Carducci MD, Nichol GS, Walker FA. Models of the Cytochromes: Crystal Structures and EPR Spectral Characterization of Low-Spin Bis-Imidazole Complexes of (OETPP)Fe(III) Having Intermediate Ligand Plane Dihedral Angles. Inorg Chem. 2006; 45:5417–5428. [PubMed: 16813405]

59. Tezcan FA, Winkler JR, Gray HB. Effects of Ligation and Folding on Reduction Potentials of Heme Proteins. J Am Chem Soc. 1998; 120:13383–13388.
60. Wen X, Bren KL. Suppression of Axial Methionine Fluxion in *Hydrogenobacter Thermophilus* Gln64Asn Cytochrome *c*-552. Biochemistry. 2005; 44:5225–5233. [PubMed: 15794659]
61. Fraser JS, van den Bedem H, Samelson AJ, Lang PT, Holton JM, Echols N, Alber T. Accessing Protein Conformational Ensembles Using Room-Temperature X-Ray Crystallography. Proc Natl Acad Sci US A. 2011; 108:16247–16252.
62. Fraser JS, Clarkson MW, Degnan SC, Erion R, Kern D, Alber T. Hidden Alternative Structures of Proline Isomerase Essential for Catalysis. Nature. 2009; 462:669–U149. [PubMed: 19956261]
63. Liptak MD, Wen X, Bren KL. NMR and DFT Investigation of Heme Ruffling: Functional Implications for Cytochrome *c*. J Am Chem Soc. 2010; 132:9753–9763. [PubMed: 20572664]
64. Williams RJP. Energized (Entatic) States of Groups and of Secondary Structures in Proteins and Metalloproteins. Eur J Biochem. 1995; 234:363–381. [PubMed: 8536678]
65. Banci L, Bertini I, Bren KL, Gray HB, Sompornpisut P, Turano P. Solution Structure of Oxidized *Saccharomyces cerevisiae* Iso-1-Cytochrome *c*. Biochemistry. 1997; 36:8992–9001. [PubMed: 9220987]
66. Fetrow JS, Baxter SM. Assignment of N-15 Chemical Shifts and N-15 Relaxation Measurements for Oxidized and Reduced Iso-1-Cytochrome *c*. Biochemistry. 1999; 38:4480–4492. [PubMed: 10194370]
67. Timkovich R, Cai ML. Investigation of the Structure of Oxidized *Pseudomonas aeruginosa* Cytochrome *c*-551 by NMR - Comparison of Observed Paramagnetic Shifts and Calculated Pseudocontact Shifts. Biochemistry. 1993; 32:11516–11523. [PubMed: 8218218]
68. Xia B, Volkman BF, Markley JL. Evidence for Oxidation-State-Dependent Conformational Changes in Human Ferredoxin from Multinuclear, Multidimensional NMR Spectroscopy. Biochemistry. 1998; 37:3965–3973. [PubMed: 9521718]
69. Morales R, Charon MH, Kachalova G, Serre L, Medina M, Gomez-Moreno C, Frey M. A Redox-Dependent Interaction between Two Electron-Transfer Partners Involved in Photosynthesis. Embo Reports. 2000; 1:271–276. [PubMed: 11256611]
70. Asciutto EK, Madura JD, Pochapsky SS, OuYang B, Pochapsky TC. Structural and Dynamic Implications of an Effector-Induced Backbone Amide cis-trans Isomerization in Cytochrome P450(cam). J Mol Biol. 2009; 388:801–814. [PubMed: 19327368]
71. Pochapsky TC, Kostic M, Jain N, Pejchal R. Redox-Dependent Conformational Selection in a $Cys_4Fe_2S_2$ Ferredoxin. Biochemistry. 2001; 40:5602–5614. [PubMed: 11341825]
72. Paixao VB, Vis H, Turner DL. Redox Linked Conformational Changes in Cytochrome *c*(3) from *Desulfovibrio desulfuricans* ATCC 27774. Biochemistry. 2010; 49:9620–9629. [PubMed: 20886839]
73. Morgado L, Bruix M, Londer YY, Pokkuluri PR, Schiffer M, Salgueiro CA. Redox-Linked Conformational Changes of a Multiheme Cytochrome from *Geobacter sulfurreducens*. Biochem Biophys Res Commun. 2007; 360:194–198. [PubMed: 17583674]
74. Whittaker M, Bergmann D, Arciero D, Hooper AB. Electron Transfer During the Oxidation of Ammonia by the Chemolithotrophic Bacterium *Nitrosomonas Europaea*. Biochim Biophys Acta. 2000; 1459:346–355. [PubMed: 11004450]
75. Arciero DM, Hooper AB. A Di-Heme Cytochrome *c* Peroxidase from *Nitrosomonas europaea* Catalytically Active in Both the Oxidized and Half-Reduced States. J Biol Chem. 1994; 269:11878–11886. [PubMed: 8163487]
76. Antonyuk SV, Han C, Eady RR, Hasnain SS. Structures of Protein-Protein Complexes Involved in Electron Transfer. Nature. 2013; 496:123–126. [PubMed: 23535590]
77. Can M, Zoppellaro G, Andersson KK, Bren KL. Modulation of Ligand-Field Parameters by Heme Ruffling in Cytochromes *c* Revealed by EPR Spectroscopy. Inorg Chem. 2011; 50:12018–12024. [PubMed: 22044358]
78. Zoppellaro G, Teschner T, Harbitz E, Schuenemann V, Karlsen S, Arciero DM, Ciurli S, Trautwein AX, Hooper AB, Andersson KK. Low-Temperature EPR and Mössbauer Spectroscopy of Two Cytochromes with His-Met Axial Coordination Exhibiting HALS Signals. ChemPhysChem. 2006; 7:1258–1267. [PubMed: 16688708]

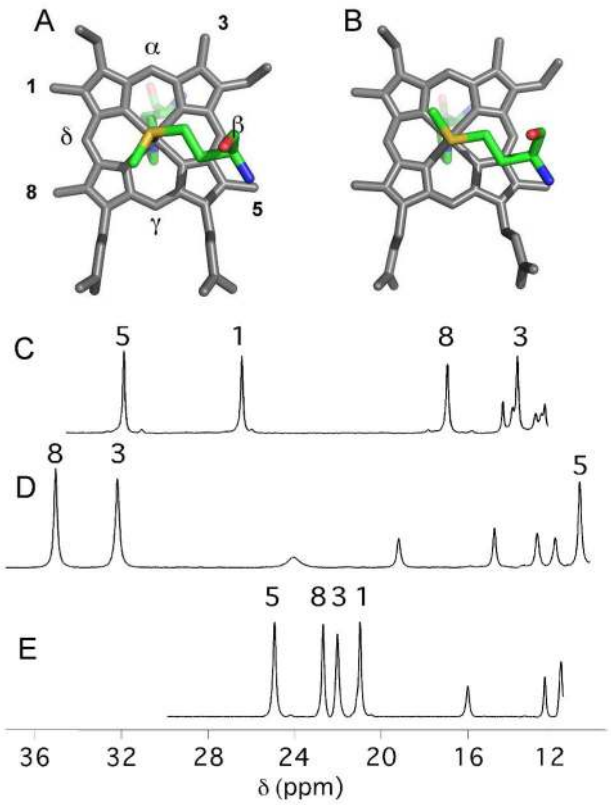

Figure 1.

A) Heme from *Pa* cyt c^4 with axial His (background) and Met (foreground) ligands highlighted, with Met in the *S* configuration, and heme methyl and meso nomenclature shown. B) Heme and axial ligands from horse cyt c^{41} with Met in the *R* configuration. C) – E) High-frequency regions of ^{1}H NMR spectra[39] of oxidized *Pa* cyt *c* (C), horse cyt *c* (D), and *Ne* cyt *c* (E), with heme methyls labeled. Heme methyl 1 is buried in the diamagnetic region for horse cyt *c*. Note that the chemical shifts in E) are approximate averages of shifts in C) and D).

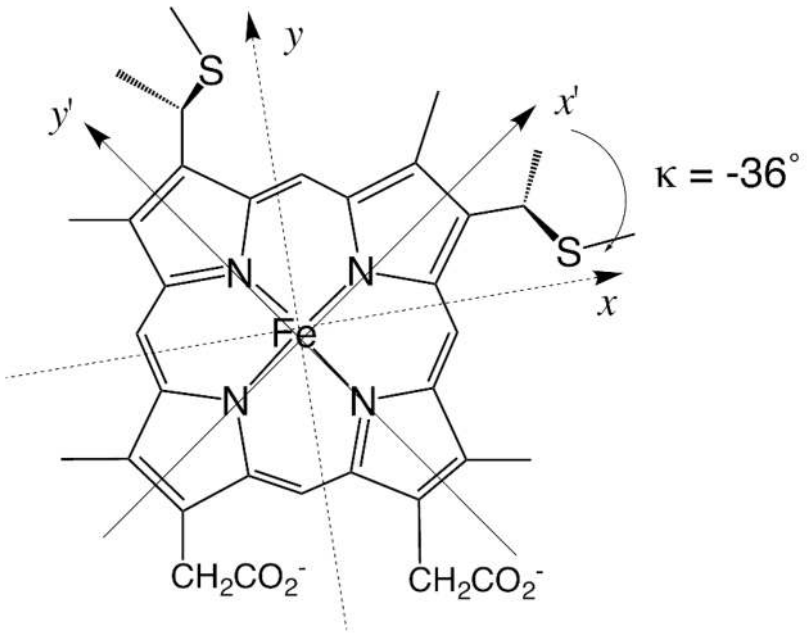

Figure 2.

Orientation of magnetic axes in *Ne* cyt *c*. The solid arrows indicate the axes in the molecular reference frame (x', y', z'), and the dashed arrows are the magnetic axes (x, y, z), where x indicates the orientation of χ_{xx}. The z' and z axes point in the direction of the viewer. The value of κ is shown (see text). In this view, the plane of the axial His ring, shown in Figure 1, approximately bisects the x' and y' axes.

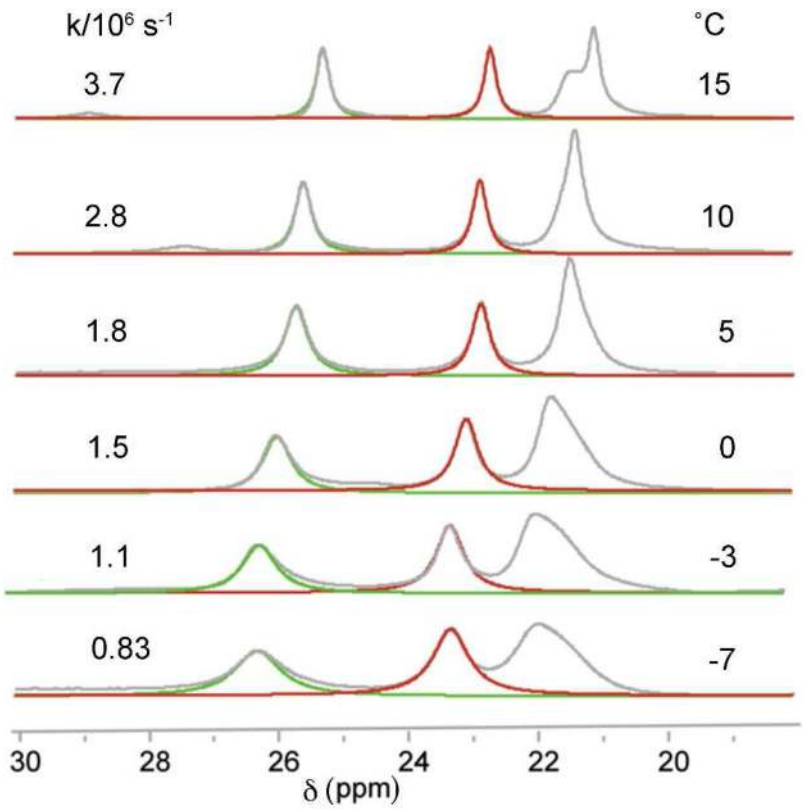

Figure 3.

WINDNMR simulation of the heme methyl ^{1}H NMR resonances for oxidized *Ne* cyt *c* in 20% methanol/80% 50 mM NaP_i pH 7. The experimental spectra are in gray and the simulated peaks for the heme 5-CH_3 and 8-CH_3 are in green and red, respectively. The 3-CH_3 and 1-CH_3 resonances were not simulated because of overlap. The rate constants determined are shown. The corresponding Eyring plot is in Figure S1.

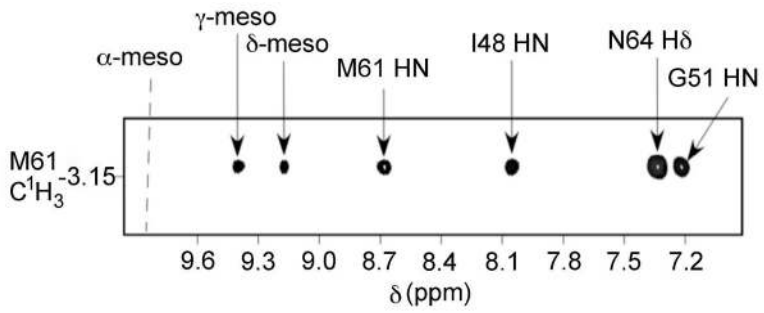

Figure 4.

Portion of NOESY spectrum of reduced *Ne* cyt *c* showing NOE cross peaks to the axial Met ε-CH_3 (−3.13 ppm). The presence of cross peaks to the heme γ- and δ-meso protons but not to the α-meso (chemical shift shown with dashed line) define the Met orientation as shown in Figure 1A.

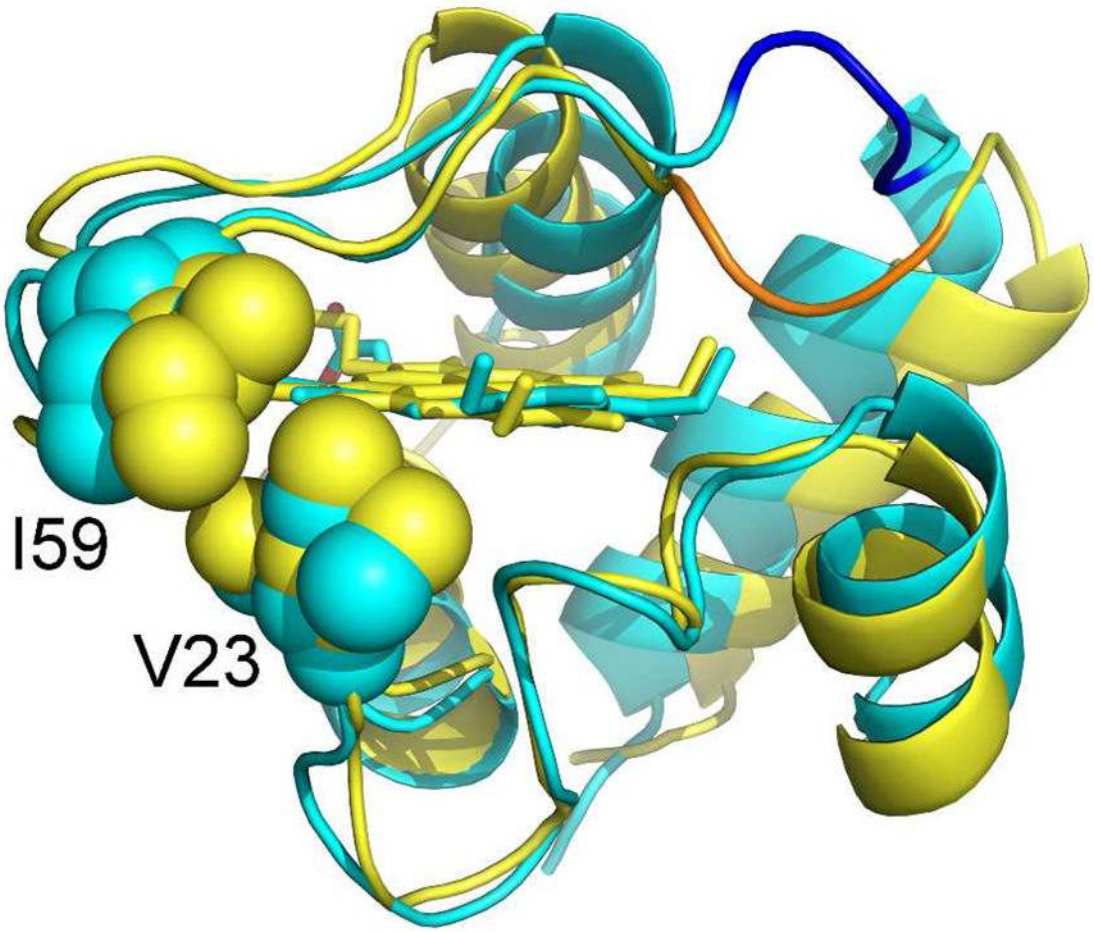

Figure 5.
Alignment of backbone atoms of the X-ray crystal structure of oxidized *Ne* cyt *c* in cyan (PDB: 4JCG)[43] and the NMR structure of reduced *Ne* cyt *c* in yellow (PDB: 1A56).[42] The backbone atoms of residues 65–67 are shaded blue (oxidized) and orange (reduced). Residues 23 and 59 are shown in space-filling mode.

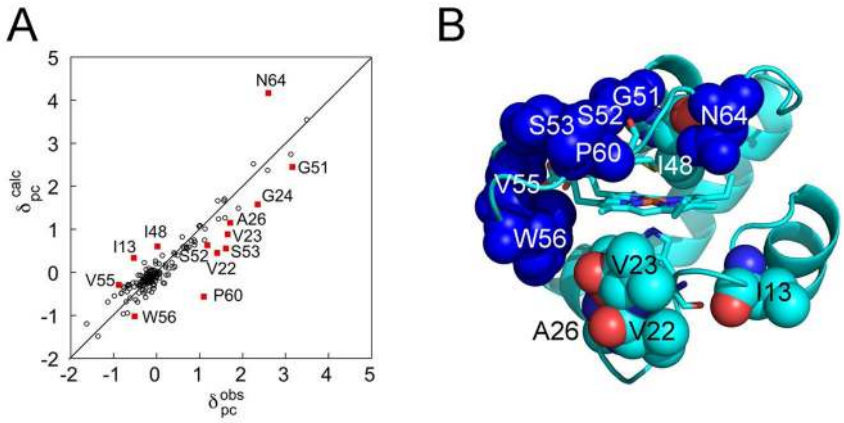

Figure 6.

A) Plot of calculated vs. measured pseudocontact shifts for *Ne* cyt *c*. Residues showing large differences (> 0.5 ppm) between calculated and measured values are labeled and denoted with red squares. B) Structure of *Ne* cyt *c* (PDB: 4JCG) with residues noted in (A) shown in spacefilling mode. Residues on loop 3 are highlighted in dark blue. The heme and its axial ligands are shown in stick mode. Gly24 is obscured by residues 22 and 23.

Table 1

Results of magnetic axes determination for *Ne* cyt *c*, compared to results for *Pa* cyt *c*[21]

Protein	β	κ	$\Delta\chi_{ax}$ (1×10^{32} m^3)	$\Delta\chi_{rh}$ (1×10^{32} m^3)	$\Delta\chi_{rh}/\Delta\chi_{ax}$
Ne cyt *c*	−13.5°	−36°	2.96	−0.40	0.13
Pa cyt *c*	5°	−12°	2.98	−1.13	0.38